Materials & Design 260 (2025) 115032

Contents lists available at ScienceDirect

Materials & Design

journal homepage: www.elsevier.com/locate/matdes

Impact of triaxiality on material behaviour characterization in hot forging processes: focus on near solidus forming

Muhammad Sajjad [a,1,*], Julen Agirre [a,2], Gorka Plata [a,3], Jokin Lozares [b,4], Carl Slater [c,5], Joseba Mendiguren [a,6]

[a] Mondragon Unibertsitatea, Faculty of Engineering, Mechanics and Industrial Production, Loramendi 4, Mondragon 20500 Gipuzkoa, Spain
[b] Hüttenes-Albertus Chemische Werke GmbH, (Vizcaya), Amorebieta, Spain
[c] WMG, University of Warwick, 6 Lord Bhattacharyya Way, Coventry CV4 7AL, United Kingdom

ARTICLE INFO

Keywords:
Near-Solidus Forming (NSF)
42CrMo4 material
FORGE NXT®
Hansel-Spittel model
Digital twin
Sustainable manufacturing

ABSTRACT

This study investigates the deformation behaviour of 42CrMo4 steel at high temperatures and varying strain rates, focusing on the impact of different deformation states (compression vs. shear) on material behaviour. Through detailed material characterization, including plane strain compression and traditional compression tests, we reveal that at temperatures between 1300 °C and 1370 °C and strain rates of 1 s^{-1}–10 s^{-1}, the material's behaviour remains largely unaffected by the deformation state. A key finding is that models based solely on compression tests can accurately predict material behaviour under plane strain conditions. Despite this, challenges persist in developing shear test geometries that can reliably capture pure shear deformation states for high-temperature applications. This research provides valuable material parameters for numerical simulations, especially in high temperature forging processes, contributing to the advancement of sustainable manufacturing technologies. These insights are crucial for optimizing processes like NSF forging, directly impacting the digital twin modelling of industrial operations and supporting the transition towards sustainable manufacturing.

1. Introduction

Near-Solidus Forming (NSF) is a specialized high-temperature hot forging process that facilitates the material flow leading to reduced forces and high material utilization. This process closely resembles closed-die extrusion, wherein the material is shaped within constrained geometries, leading to improved dimensional accuracy and reduced porosity. A global description of the process can be found in the work of Zoqi et al. [1], whereas a detailed description of the process can be found in the contribution of Lozares et al. [2] for an automotive component. NSF presents significant advantages over conventional hot forging, including lower flow stresses, enhanced formability, and the ability to produce complex components with superior mechanical properties as stated by [2] in which a decrease of necessary material by 20 % and a reduction of forces up to ¼ were achieved. These benefits make NSF particularly attractive for industries such as aerospace and automotive, where precision and performance are crucial.

To optimize NSF and other high-temperature forming processes, Finite Element Method (FEM) simulations play a pivotal role in manufacturing process design and setup. FEM enables in-depth analysis of stress, strain, and temperature distributions during deformation, allowing manufacturers to fine-tune process parameters and predict potential defects before physical trials, as shown by Abedul et al. [3] in their work on duplex stainless steel cutting process. By integrating material properties, thermal gradients, and contact conditions, FEM enhances process efficiency, reduces production costs, and minimizes

* Corresponding author.
E-mail addresses: msajjadk91@gmail.com (M. Sajjad), jagirreb@mondragon.edu (J. Agirre), gplata@mondragon.edu (G. Plata), jokin.lozares@ha-group.com (J. Lozares), C.D.Slater@warwick.ac.uk (C. Slater), jmendiguren@mondragon.edu (J. Mendiguren).
[1] 0000-0002-4897-079X
[2] 0000-0002-6361-5358
[3] 0000-0003-4606-8185
[4] 0000-0002-8879-5762
[5] 0000-0002-7491-4919
[6] 0000-0002-2912-9030

https://doi.org/10.1016/j.matdes.2025.115032
Received 12 June 2025; Received in revised form 28 September 2025; Accepted 27 October 2025
Available online 30 October 2025

material waste, as shown by Sajjad et al. on their sensitivity analysis with three industrial benchmarks manufactured by NSF [4].

However, FEM models for high-temperature forming processes are inherently complex, requiring numerous input parameters and hypotheses regarding material behaviour, frictional interactions, and thermal effects. This complexity often amplifies the uncertainty in simulations, particularly when extrapolating material data obtained under limited stress states. The effect of the strain rate was studied by Roth and Mohr [5], while Sajjad et al analysed the impact of the friction coefficient [6] and heat transfer coefficient [7] in hot forming operations. These complexities make the accurate representation of material response a challenging task. Despite the advanced numerical techniques available, state-of-the-art FEM models for NSF still exhibit inaccuracies, leading to deviations between simulations and experimental results as concluded by Plata et al. [8] and Slater at al. [9].

Some authors assure that a key factor contributing to these discrepancies is the material characterization methodology used in high-temperature forming processes [8]. In most cases, material data for FEM models is obtained from compression tests performed at elevated temperatures, as used by Park et al. in order to calibrate Hosford-Coulomb model for EH36 grade high tensile strength [10]. While this approach is standard practice, recent studies suggest that deformation during NSF and similar hot forging processes often involves significant shear components due to the material's flow characteristics within a closed die [8,9]. This raises a fundamental question: do materials behave differently under shear deformation at high temperatures compared to compression? If material models are identified based solely on compression tests, can they reliably predict behaviour in high temperature conditions when shear deformation dominates? This question is particularly relevant, as several recent studies have shown that deformation-state sensitivity can significantly affect flow stress and microstructural evolution, leading to deviations in model predictions when applied beyond the calibration conditions [11].

Different mechanical testing methodologies are employed to characterize material response under various stress states, as illustrated in Fig. 1. Sample geometries are designed to impose distinct stress triaxiality and Lode angle conditions. Samples range from uniaxial compression (negative triaxiality and lode angle, as presented by Lou et al. on their study of DP980 steel sheets and aluminium alloy AA7075 [12], to uniaxial tension, with positive triaxiality and lode angle, in whereas example can be found in Roth et al. work [13] on aluminium alloy AlSi10Mg during testing and modelling. In between, plane strain compression, with zero lode angle and negative triaxiality, has been widely used for characterization in forming, as presented by Chen et al. [14] for the characterization of aluminium alloy AA5052 specimens. For close to pure shear testing (zero triaxiality and lode angle) a variety of testing samples have been proposed in literature, from the cup shape sample of the Hor et al [15] and the simple specimen of Zhang et al. [16], to the butterfly shape samples of Gorji et al. [17] and Kameneh et al. [18] among others. Further modification to the initial shear samples can be found in the work of Andrade et al [19] and Mehari et al [20].

Both stress triaxiality and Lode angle are widely used to represent the stress state in which a shear deformation mode corresponds to stress states surrounding the zero values of both quantities (a detailed description of deformation-states can be found in the work of Driemeier et al. [21]). These concepts have been extensively used in fracture mechanics as stress triaxiality, and lode angle highly influence void nucleation, growth, and ductile fracture. This was stated by Rice and Tracey [22] and McClintock [23] in their early works in the 1960 s and has been widely studied by other authors such as Rickhey et al. [24] among others. Nevertheless, as recently stated by Mohr (D. Mohr, personal communication, February 20, 2025) it has not to be confused between 'shear dominated fracture' and 'shear dominated deformation'. In the former one the final stretch of the deformation, near the fracture of the material, is under shear conditions while in the later one the deformation path itself is shear dominated while the fracture can deviate from that condition.

Several studies have conducted in-depth investigations into the evolution of stress triaxiality of the fracture are during deformation tests mainly oriented towards a defined fracture point stress-state and not that much focus on the deformation path of the sample as a whole. Advanced techniques such as Digital Image Correlation (DIC) and finite element simulations have provided insights into how triaxiality varies across different regions of the specimen during testing as shown by Roth et al [13] for the SLM AlSi10Mg, or Zhang et al. [25] for the 7075 aluminium alloy among others. For instance, Li et al. demonstrated that in high-temperature tensile tests, stress triaxiality evolves dynamically,

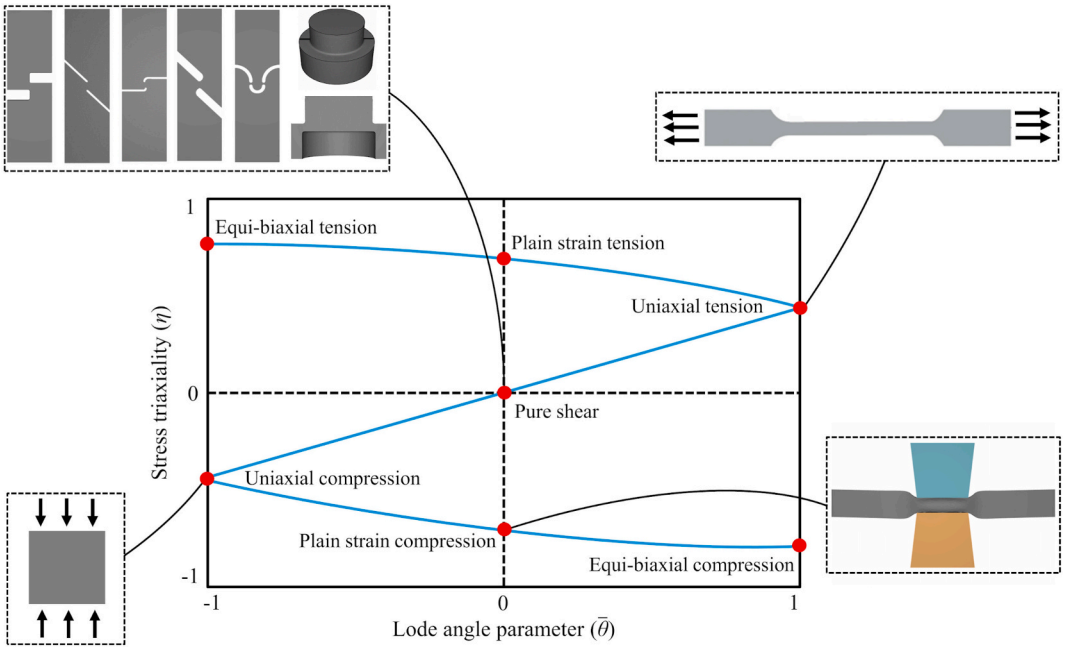

Fig. 1. Stress states on the stress triaxiality and Lode angle parameter space.

correlating with strain localization and failure patterns [26]. This evolving nature of triaxiality further complicates material characterization and raises questions about the accuracy of compression-based material models for predicting NSF behaviour. Consequently, incorporating multiple loading paths, or at least validating compression-based models against alternative stress states, becomes crucial to ensure predictive reliability in near-solidus forming processes [27].

These insights highlight the limitations of relying exclusively on a single deformation mode for material characterization at elevated temperatures. While compression tests remain the most widely adopted due to their simplicity and stability, they do not fully capture the complexity of deformation-state sensitivity observed in high-temperature forming [28]. In particular, the interplay of stress triaxiality, strain localization, and rapid thermal softening near the solidus point suggests that alternative loading paths may reveal markedly different responses. Thus, a systematic investigation into how various specimen geometries promote distinct deformation-states is necessary to clarify the applicability of compression-based models in broader forming conditions.

Given these considerations, the present study aims to give answer to the following open questions: ① what is the predominant/driving deformation-state for each state-of-the-art material characterization samples? ② do materials (specially 42CrMo4 steel) behave differently under shear deformation at high temperatures compared to compression; and therefore, material models identified based solely on compression tests, can they reliably predict behaviour in high temperature conditions when other deformation-states dominates?

For the sake of clarity, the manuscript is organized in two separate chapters, one for each question. The first chapter addresses the predominant/driving deformation-state of the state-of-the-art material characterization samples. In this regard, finite element models will be used to replicate the testing samples and study the triaxiality evolution of the whole sample during the test.

The second chapter addresses the impact of the deformation-state in the material characterization. To do so, the prediction accuracy of the plane strain compression FEM model, fed with a material model characterised with compression test data, will be used. This will clarify the potential impact of the characterization stress state for the conditions under study.

2. State-of-the-art characterization samples predominant deformation-state

Following a classic scientific structure, the chapter is organized as methodology, results and discussion and conclusions. In this section the first question will be studied: ① *what is the predominant/driving deformation state for each state-of-the-art material characterization samples?*

2.1. Research methodology

As stated by Mohr (D. Mohr, personal communication, February 20, 2025) it has not to be confused between predominant/driving deformation-state during a test, and the particular state in which the fracture has been achieved. When deforming a sample (applicable to any geometry of study Fig. 1) each area/point of the sample contributes to the overall deformation energy. Taking the tensile test of Fig. 1 as example, as it is well known, the area/points in the calibrated neck of the sample will deform under uniaxial tensile deformation-state. Nevertheless, the material in the 'heads' of the sample will also deform, under different strain configuration (different triaxiality), but with a neglectable contribution to the overall sample deformation energy as most of the deformation will happen in the weekend calibrated neck. Therefore, we can state that when we characterise a material with that sample shape, the force that is measured is generated with the contribution of uniaxial tensile response of the material.

On the contrary, with geometries more focused on the state in which the fracture is achieved (pure shear samples of Fig. 1 for example) it is uncertain what is the overall contribution of the points/zones under pure shear to the global deformation energy and therefore to the measured force.

In this context, this section of the manuscript will analyse, with the use of a numerical representation of each sample, the contribution of each point and each deformation-state to the overall deformation energy. Finite element representations of the sample will be used to track the deformation-state of each point and its contribution to the overall output. Fig. 2 shows a schematic representation of the methodology to be followed to visualise the contribution of each deformation-state to the overall deformation energy. FORGE NXT® software with reference 42CrMo4 material, from the software database, will be used to represent each sample (a more detailed description of each model will be added for each sample in a subsequent subsection). Hansel–Spittel model is employed, characterising the flow stress as a function of strain, strain rate, and deformation temperature, further details available in the work of Sajjad et al. [29].

As shown in Fig. 2 the triaxiality (as a value that represents the deformation-state) of each integration point will be tracked and represented against the accumulated plastic strain (refer to [30] for a detailed description of the accumulated plastic strain formulation). The accumulated plastic strain (plastic strain hereafter) will be taken as a representative of the deformation energy. Meaning that points with lower plastic strain are not really contributing much to the overall plastic energy and therefore to the force, while points with high plastic strain contribute more towards the resulting force. Therefore, assuming that each integration point represents more or less the same volume quantity, the higher concentration of points in a higher plastic strain area will represent the predominant deformation-state.

In the following lines a detailed description of the methodology particular of each sample is presented, covering: compression test, plane strain compression test, and seven different shear test samples.

2.1.1. Compression test

The compression test is a widely recognized method for assessing the mechanical properties of materials. A sample of 10 mm in diameter and 15 mm in length is used in this study. An initial homogeneous temperature of 1375 °C (classic NSF temperature) is assumed in the sample. From the modelling side, the sample is treated as a deformable solid while the top and bottom dies are considered rigid due to the large difference in deformation between both entities. A schematic representation of the simulation can be seen in Fig. 3.

A unilateral contact condition and a friction coefficient at the part/die interface were defined based on findings from the previous studies of the authors [6]. Heat transfer between the parts and dies, as well as

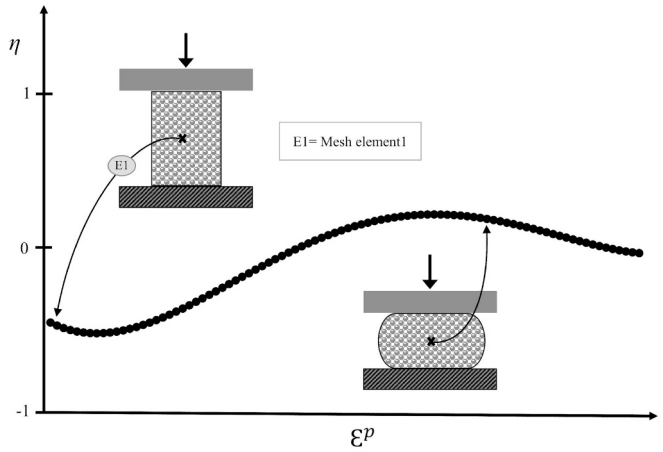

Fig. 2. Stress triaxiality of the deforming elements with respect to plastic strain.

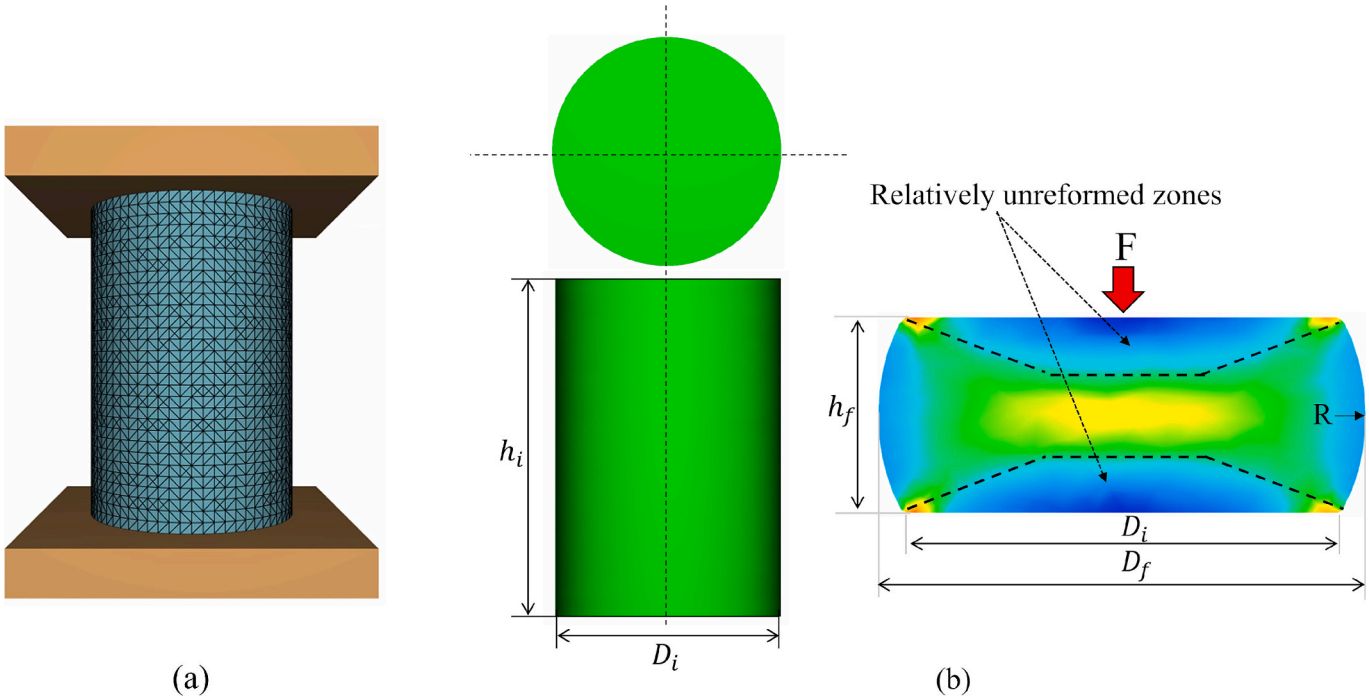

Fig. 3. Model of compression test, specimen before (a) meshing (b) deformation.

between the parts and the surrounding air, is simulated using a uniform thermal conductivity value of 800 and 10 W/m^{2}K respectively under all test conditions [7]. The dies were set to a temperature of 250 °C as per usual boundary conditions in the characterization tests. The lower die was kept stationary while a specified vertical displacement derived from experimental tests, is assigned to the upper die. Finally, a mesh size of 0.5 mm is utilized with the remeshing rule to future enhance the simulation results.

2.1.2. Plane strain compression test

In the plane strain compression test (Fig. 4), the material undergoes deformation under compressive loading. Leading, at least in theory, to plane strain conditions between the dies. In this study, a rectangular specimen measuring 140 mm x 20 mm with a thickness of 10 mm is subjected to compressive forces along its axis with an assumed initial temperature of 1375 °C.

Following the same strategy as in the compression test, dies were assumed rigid, while considering the specimen as a deformable body. To further enhance the accuracy, the billet was meshed heterogeneously as illustrated in Fig. 4(b). Specifically, the centre part of the billet was finely meshed due to higher anticipated deformation, while coarser elements were used on the remaining sides to balance simulation time and accuracy. This meshing approach was refined through a trial-and-error process to balance simulation time and maintain the required accuracy of the results. Moreover, identical boundary conditions for the heat transfer coefficient and friction coefficient were applied, as characterized by Sajjad et al. during the sensitivity analysis of the NSF process [6,7].

2.1.3. Shear test

Various sample geometries aimed at characterizing material behaviour under pure shear conditions can be found in the literature [5,13]. It has to be considered that most of them (Fig. 5 from SH1 to SH6) are designed having the particular state in which the fracture has been achieved in mind and not considering the predominant/driving deformation-state during a test [5,16,17,19,20]. In contrast, the seventh sample (SH7), presented by Hor et al. is specifically designed for forging material characterization under shear deformation-state [15].

Samples SH1 to SH6 have a base plate thickness of 10 mm and a width of 30 mm in this study. Sample SH7 has a thinner diameter of 12.6 mm, an external diameter of the thick part of 18 mm, and an internal diameter of 13.6 mm. For more detailed geometrical specifications, please refer to the original references [5,16,17,19,20] for the SH1 to SH6 samples and [15] for SH7 sample).

Following the same strategy as before, only the samples are assumed as deformable. All samples have a very narrow area in where theoretically the shear deformation is concentrated (the overall deformation as well), that is why a heterogeneous mesh is distributed in the sample in

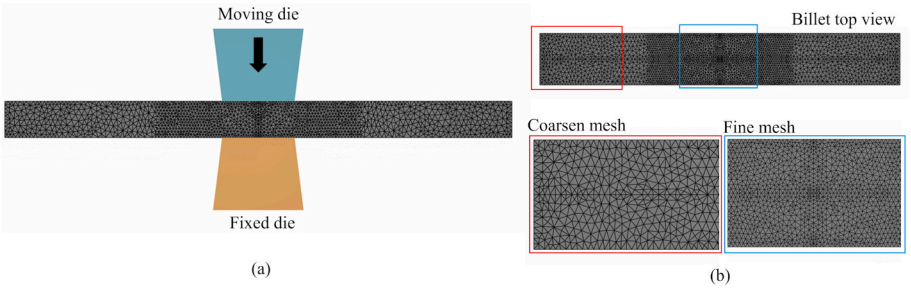

Fig. 4. Numerical modelling of the plane strain compression test.

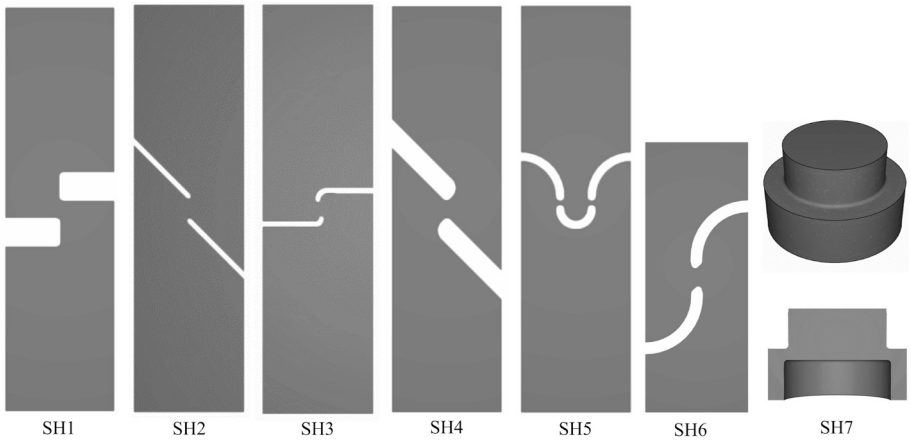

Fig. 5. Shear test samples specification.

where a finer mess of 0.4 mm is applied in the refined area and a coarse mesh (1 mm) in the sample holding area. Fig. 6 shows the mesh distribution for SH1 as an example of the mesh distribution.

In order to represent the testing reality as close as possible, two distinct heating strategies are used in these samples. The seventh geometry, SH7, is assumed to be heated in a furnace (same as previous samples) and therefore simulated with an initial temperature of 1375 °C. On the contrary, previous experience of the authors [8] had led to the necessity of developing a different heating strategy for samples SH1 to SH6.

Often, these samples (when testing at high temperatures) are heated using a Joule heating system. However, due to the non-axisymmetric shape of the sample a heterogeneous temperature distribution is generated by the Joule currents [8]. That is why, for these samples, the heating phase has been also simulated to consider the adequate temperature distribution through the sample.

The Joule heating process is simulated in Multiphysics COMSOL software, resulting in the heterogeneous temperature distribution illustrated in Fig. 7(left). Subsequently, the temperature field, which exhibits a rounded distribution (Fig. 7, centre), is transferred to FORGE NxT® software to serve as the initial temperature distribution for the testing phase. Following this, shear simulations are conducted in FORGE NxT® to evaluate the deformation-state.

2.2. Results and discussion

Once the numerical methodology of each sample is presented, in the following lines the results of triaxiality against plastic energy for each sample is presented. In addition, a deeper discussion of the finding is conducted.

2.2.1. Compression test results

For the sake of simplicity results at two different scales will be presented. On the one hand, three arbitrary points will be selected (defined as S1, S2 and S3 in Fig. 8a) and the evolution of their triaxiality during the deformation process will be evaluated (Fig. 9a). Even if the points are selected to high deformation areas, in this result visualization no magnitude of the plastic strain is presented as the only intent is to analyse the evolution or stability of the triaxiality value during the deformation.

On the other hand, a more massive data analysis will be conducted. In this case the whole deformation body (points of the whole sample, shown in Fig. 8b) will be considered and the pair data of triaxiality and plastic strain of every point will be plotted. To give an idea of the evolution of the triaxiality, ten steps across the total 9.5 mm stroke will be overplotted in the same graph. As expected, when increasing the stroke, the plastic strain of the points will increase. In this view, it will not be possible to track the triaxiality evolution of a specific point, but it will be possible to evaluate the global contribution of each deformation-state to the overall energy.

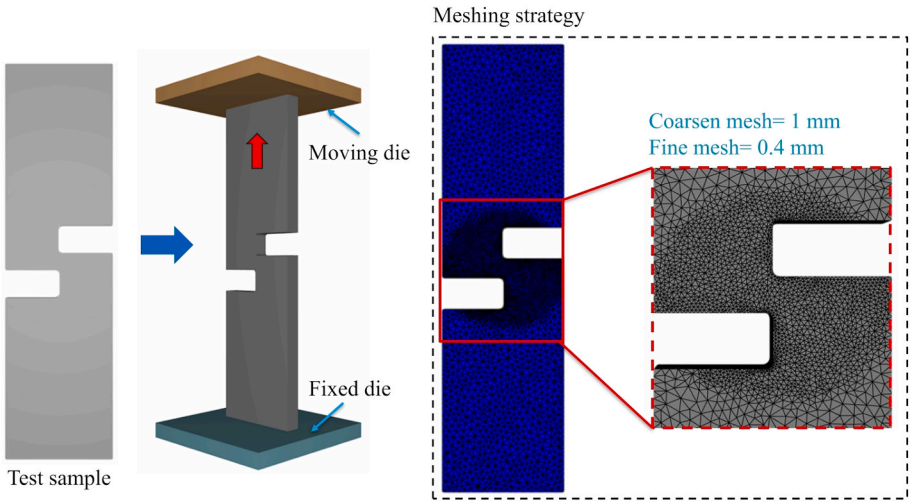

Fig. 6. Finite element modelling of SH1 (same methodology used for all shear samples).

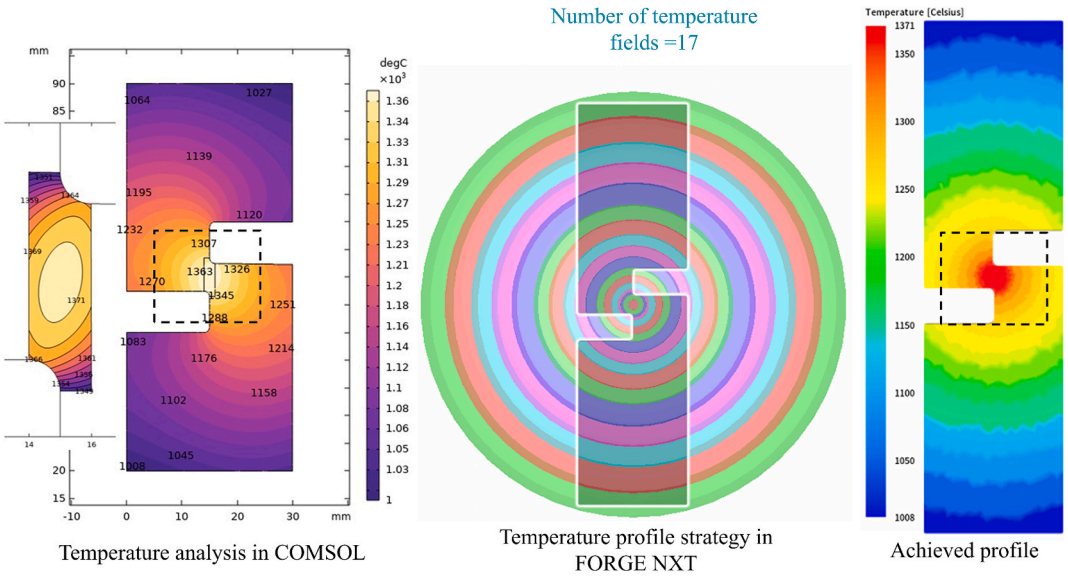

Fig. 7. Thermal characterization and optimization of the shear test boundary conditions.

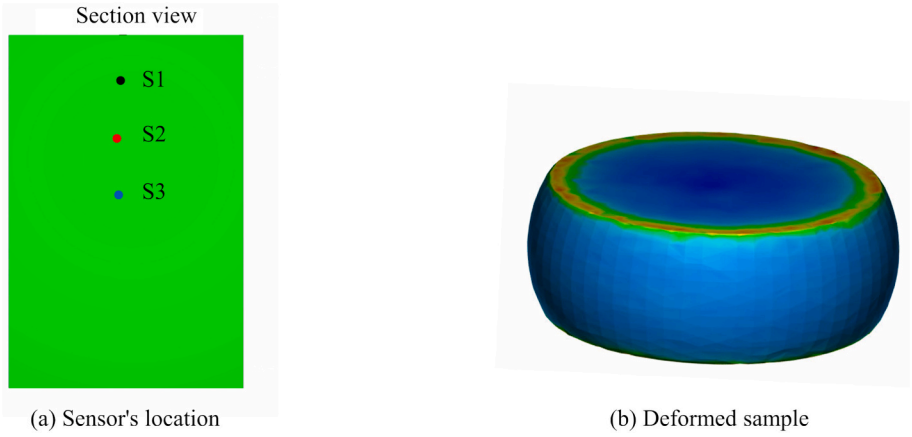

Fig. 8. Simulation results (a) sensor's location (b) compressed sample.

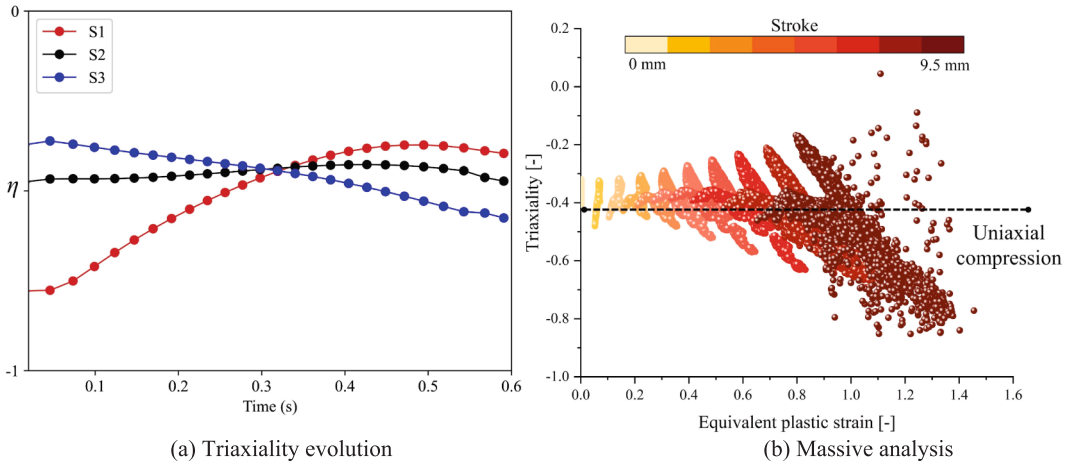

Fig. 9. Triaxiality analysis plots of the compression test.

At local level, considering the arbitrary S1 to S3 points (Fig. 9a) it's evident that at the beginning of the compression, the triaxiality value for the first point (S1 closest to the surface) starts at −0.75 and ends at −0.45. This indicates that in zones close to the contact with the dies, the material initially experiences plane strain, transitioning to uniaxial compression behaviour. In the second point (S2) pure uniaxial

compression is consistently recorded throughout the deformation stroke. Similarly, at the centre of the billet (S3), the same triaxiality behaviour is observed [31].

At the massive analysis (Fig. 9b), in order to have a reference, the black dashed line represents the expected theoretical triaxiality for the test. First, it can be clearly observed that the increase of stroke increases the plastic strain on the different points. In addition, at every increment, the dispersion of the triaxiality values also increases, augmenting the range from (−0.3 to −0.5) of the initial increment to the (−0.2–−0.8) of the last increment.

The characteristic round shape generated due to the friction during the compression test (Fig. 8b) and the test material flow leads to a major contribution of a range of triaxiality from approximately (−0.8–−0.3) in where most of the points can be found in the range of (−0.4–−0.7) with some outliers and some minor contribution of other areas. It must be also considered that the force displacement data obtained from the test will represent the deformation energy of different ranges. At the beginning of the test more points will contribute at the expected compression deformation-state and when increasing the stroke, the contribution of points with lower triaxiality levels will be more important. Therefore, if a close to compression characterization is necessary, only the early data of the deformation will be valid unless a lower fraction that leads to a more homogeneous deformation distribution in the sample is achieved.

2.2.2. Plane strain compression test results

Fig. 10 shows the deformation overview of the plane strain compression test predicted by the simulation. It can be appreciated in the figure the location of the three arbitrary points in the deformation area.

Fig. 11 shows the triaxiality evolution in the three arbitrary points (Fig. 11a) and the massive results illustration (Fig. 11b).

At triaxiality evolution level, the first noticeable difference compared to the compression test results, is the stability of the triaxiality in the three points. In addition, in a first glance (and with the accuracy of the plot) both S1 and S2 (supposedly in areas or larger deformation) follow the expected triaxiality state with a triaxiality around (−0.7). At the massive analysis result (Fig. 11b) a higher dispersion is observed with average triaxiality value ranges between −0.45 and −0.8, indicating that the deformation behaviour primarily transitions between uniaxial and plane strain compression conditions. The uniaxial compression behaviour originates from the areas in contact with the edges of the forming die, as shown in Fig. 10, where the material experiences pure compression during the deformation process. As a global trend, the range of deformation-state is maintained during the stroke and no significant variations are observed from the start of the deformation until the maximum stroke of the die. In addition, the outlier points, characterized by triaxiality values in the range (−0.1 to −0.4) appear for all stroke values but do not represent the bulk of the data.

Nevertheless, as a limitation of these results it has to be considered that as presented in Fig. 4 a heterogeneous mesh distribution has been used. Therefore, statistically, more data points will be collected from the central area of the sample compared to the 'heads' of the sample. However, from the global view on Fig. 10 one can assume (without much uncertainty) that most of the deformation energy is localized in the area with a finer mesh minimizing in this sense the potential impact of the heterogeneity of the mesh distribution.

2.2.3. Shear test results

Following the same strategy as in previous samples, a local results analysis with arbitrary points and a global observation with the massive analysis will be conducted for the seven shear test samples of Fig. 5. Fig. 12a presents the deformation field view of the seven samples in which the location of the arbitrary point is identified. For the sake of simplicity, and having seven sample geometries, only one point per sample has been analysed. In line with the heterogeneity mesh distribution discussed in the previous sample geometry, in this Fig. 12a, the concentration of the deformation at the central area is observed. This needs to be kept in mind for the discussion as an heterogeneous mesh distribution has been also used in these samples as shown in Fig. 6.

At Fig. 12b in where the evolution of the triaxiality for the different arbitrary points is presented, a steady increase of the triaxiality during the testing period is observed. All samples start with a triaxiality around pure shear (with a range of ± 0.2) and increase to the range of (+0.5 to 0.0) by the end of the test. Sample SH6 exhibits minimal variations in stress triaxiality, ranging from (−0.02 to + 0.1), while SH7 similarly shows slight variations, ranging from (−0.1 to 0.01). For the other samples, stress triaxiality starts low, averaging around (0.1) initially, but rises towards the end of the shearing phase. This suggests that the rotation of the central section when pulling from the sample deviates the deformation-state from a close to shear behaviour towards a uniaxial or sometimes plane strain condition.

A detailed analysis of the global deformation-states is presented in Fig. 13, showing the massive analysis illustration of the seven shear geometries under study. Like previous graphs, the theoretical triaxiality distribution is represented by a continuous black line.

First obvious output is that at any stroke of the testing a large variety of deformation-state occurs. This is true at least for the last stroke that masks (with bright red) previous stroke data. Then, the second observation is that even if a large variety of deformation-state is observed, overall, the largest range of triaxiality (−0.7–0.5) occurs at relatively low plastic strain values. It has to be remembered here that we are referring to plastic strain but in reality, is the 'accumulated plastic

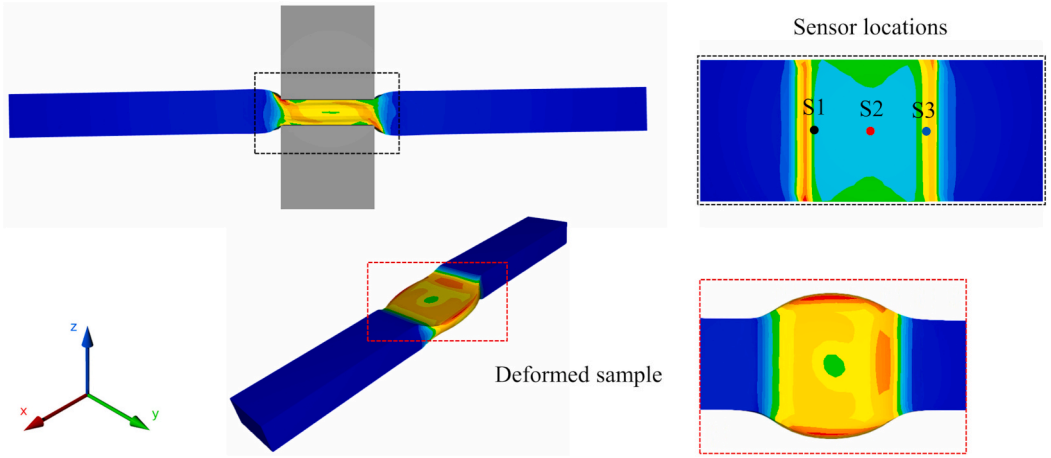

Fig. 10. Deformed plane strain compression sample with the location of the arbitrary three points.

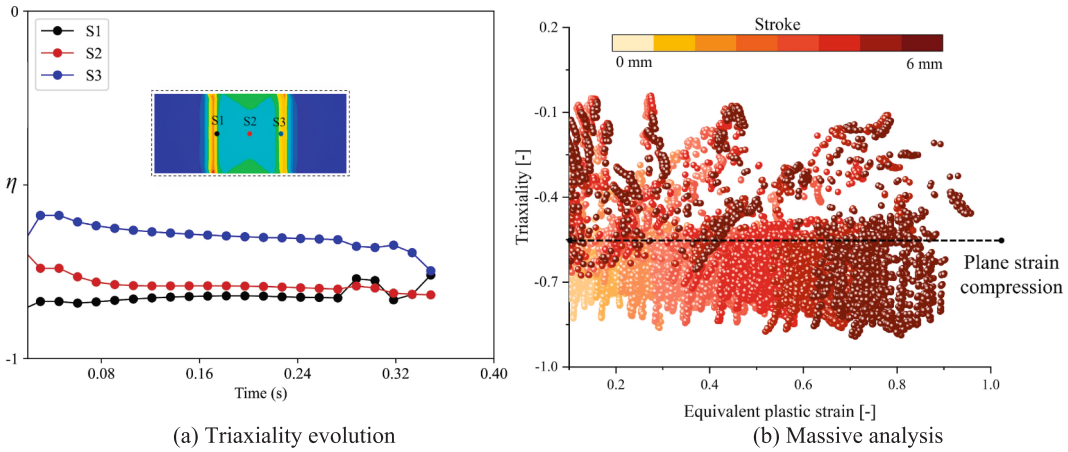

Fig. 11. Triaxiality analysis of the plane strain compression test.

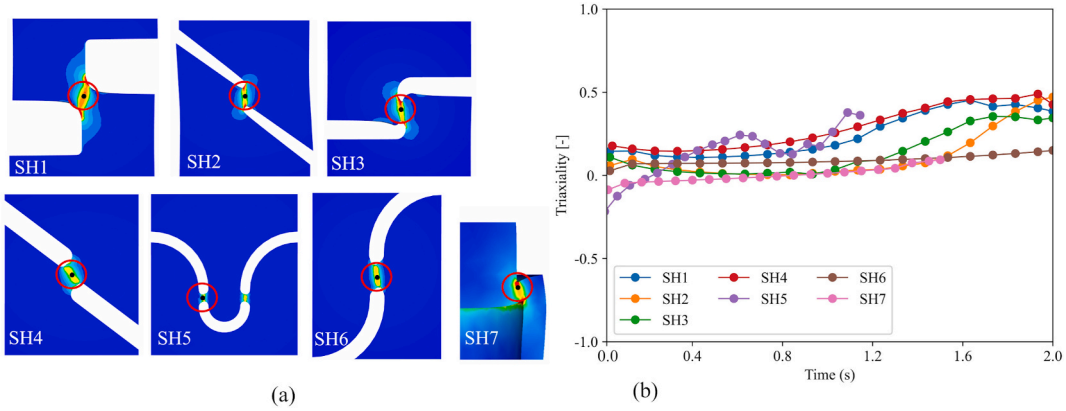

Fig. 12. Triaxiality analysis of shear samples at max deformation location (SH1-SH7); (a) arbitrary point location (b) Triaxiality evolution.

strain' and therefore, having 0.5 of accumulated plastic strain is not even close to deforming the material to a plastic strain of 0.5 in most cases. And depending on the deformation path a large value of accumulated plastic strain can be achieved.

Nevertheless, most samples, and definitely samples SH1 to SH6 exhibit a clear spike shape on the triaxiality distribution for medium to high plastic strain values. However, with the exception (and not too far from the others) of SH6, all SH1 to SH5 samples clearly show a high contribution of deformation energy from deformation-states of triaxialities ranging from (0.2 to 0.4). In the case of SH6 it is appreciated that the range is closer to (0.1–0.35) leading to a closer approximation to shear deformation-state. These results combined with the results shown in Fig. 12 conclude that the butterfly shape of the samples, could lead to specific points of fracture under shear deformation-state but it cannot be said that the predominant/driving deformation-state during a test is shear state. This is related to the fact that the calibrated neck rotates during the pulling of the specimen, switching from shear to uniaxial tensile deformation-state.

Analysing SH7 a clear difference is observed between the arbitrary point analysis and the massive analysis. The arbitrary point study (Fig. 12b) clearly shows an acceptable shear deformation-state for the central point. And this could be of a greate utility for example if microstructure evolution under shear is under study and one can focus only on that specific point. However, from the massive analysis results can be concluded that shear is not the predominant/driving deformation-state in SH7 sample.

2.3. *Conclusions of research question ①*

In this section the main conclusions of the answer to the following question are summarised: ① *what is the predominant/driving deformation state for each state-of-the-art material characterization samples?*

- *Compression Test:* The samples maintain a well-balanced compression deformation mode with a triaxiality close to −1/3 up to approximately 80 % of plastic deformation. Beyond this point, the deformation mode begins to deviate towards experiencing plane strain and equi-biaxial compression.
- *Plane Strain Compression Test:* During this test, the average triaxiality value ranges between −0.45 and −0.8. This indicates that the deformation behaviour primarily transitions between uniaxial compression (particularly at the areas in contact with the edges of the forming die) and plane strain compression conditions.
- *Pure Shear Test*: Initially, the samples exhibit a pure shear deformation mode. However, a significant contribution to the deformation energy arises from material points deforming under triaxiality values close to uniaxial (for SH1 to SH6) and values close to (−1) for SH7. This shift suggests a transition from the initial pure shear state towards a compression plane strain or equi-biaxial compression state.

These findings highlight the difference between: Samples designed to get a predominant/driving deformation-state during deformation and in this way characterize the material behaviour under that deformation-state. And samples oriented towards obtaining a specific deformation-stage at the fracture point or at one specific arbitrary point. In this

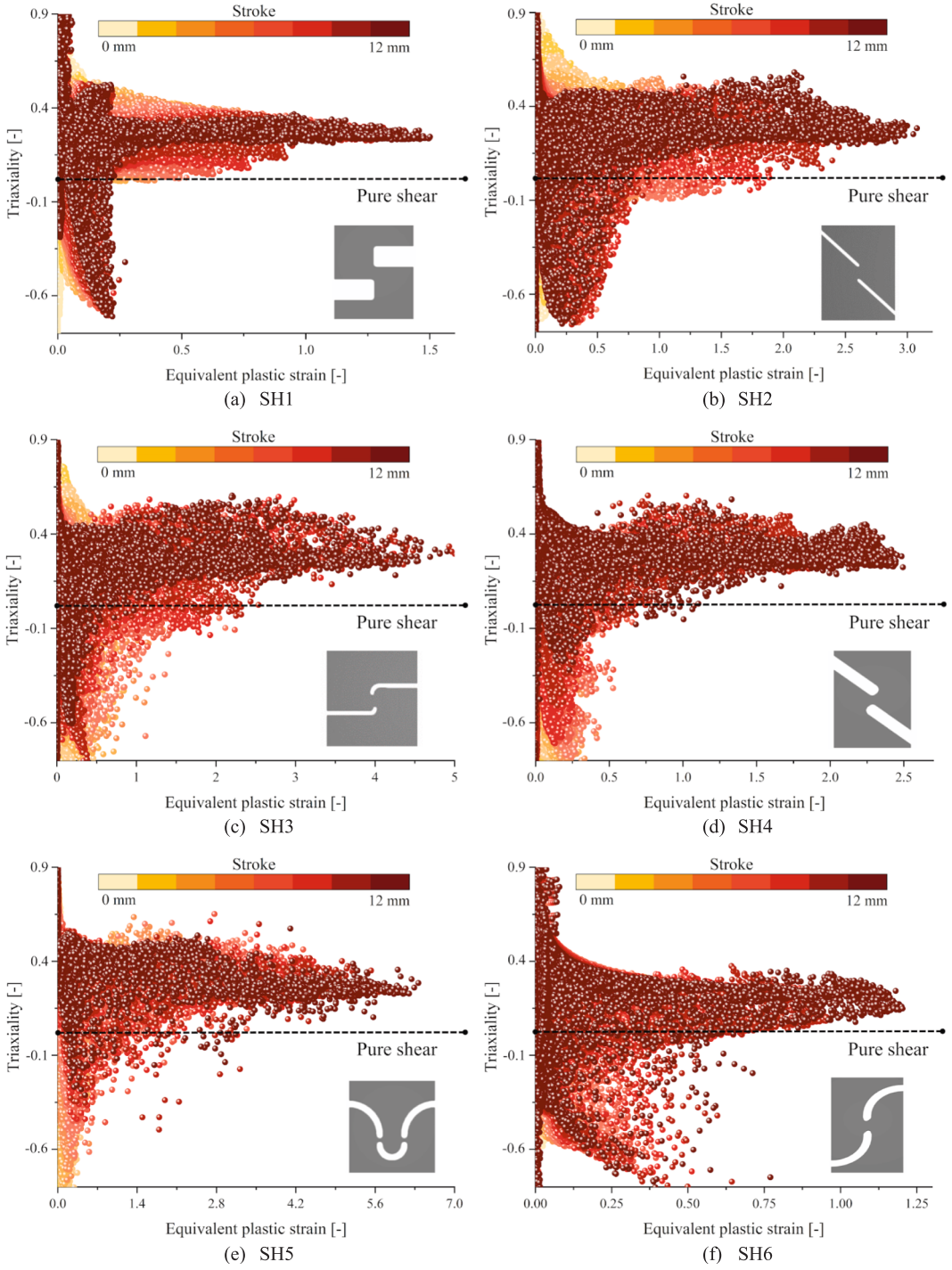

Fig. 13. Massive analysis of the shear samples (SH1-SH7).

sense, both compression and plane strain compression have been found to be acceptable solutions for material characterization whereas SH1 to SH7 shear samples do not represent the material behaviour under shear deformation-state.

In conclusion, with the state-of-the-art testing samples, only compression and plane strain compression characterizations can be conducted assuring the desired deformation-state. On the contrary, the shear samples (also including the SH7 previously used by other authors claiming shear characterization) do not represent the material behaviour under shear deformation-state and this misguiding should be avoided.

3. Influence of the deformation-state for material characterizations at high temperature

Once the first question has been answered, now is time to address the second open question: ② *do materials (specially 42CrMo4 steel) behave differently under shear deformation at high temperatures compared to compression; and therefore, material models identified based solely on compression tests, can they reliably predict behaviour in high temperature conditions when other deformation-states dominates?*

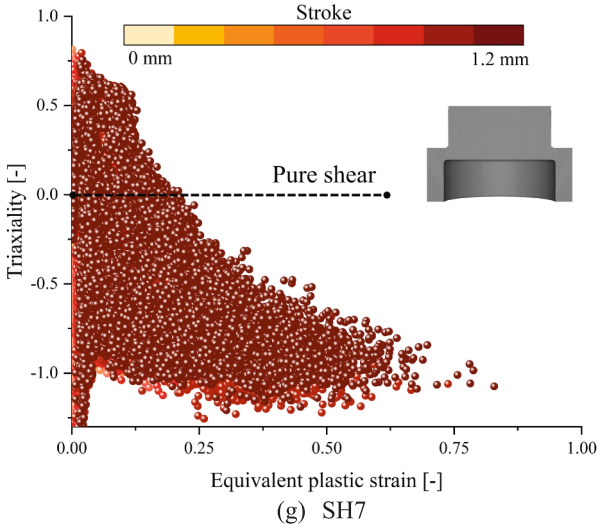

Fig. 13. (*continued*).

3.1. Research methodology

The ideal strategy to answer this question could be to characterize the material under shear deformation-state and compression deformation-state separately and compare the behaviour. However, two key findings in the process of answering question ① prevent the ideal strategy.

On the one hand, it has to be taken into account that the only way of translating the force displacement output of a material characterization test into the stress–strain (material behaviour) data is by assuming an ideal homogeneous deformation-state. In that sense, from the massive analysis of the different state-of-the-art samples has been shown that heterogeneous deformation-states are achieved in all samples. Therefore, the analytical assumptions will be introducing a critical error. Therefore, an inverse FEM identification strategy will have to be followed for material behaviour identification. A detailed description of the technique can be found in Cooreman at al. [31] or Bäker and Shrot works [32], among others. As a global description is basically a try and error strategy. First, from the experimental test, force displacement data is obtained. Then, a numerical representation of the test is constructed. This can be a simple FEM model or a more complex surface response or other advanced modelling. This numerical representation is feed with a material behaviour model. In the case of hot forging a Hansel–Spittel model is usually employed as it permits a high flexibility and strain rate, temperature and strain dependency. Next, an arbitrary set of material model parameters is chosen as a starting point, and the prediction of the numerical representation is compared to the experimental data. Typically, the first trial is a clear failure, and therefore the model parameters are iteratively modified until the numerical representation force–displacement data matches the experimental one. At that point it is assumed that the material follows the behaviour shown by the material model with the specific parameters of that iteration.

On the other hand, another critical finding of previous section (answering question ①) is that there is not state-of-the-art sample geometry that really represents the shear deformation-state as all seven studied samples have a critical contribution of other deformation-states. That is why, in this study instead of comparing compression test against shear test geometry (that we now know does not represent shear deformation mode) a comparison between compression and plane strain compression will be performed. Authors acknowledge that these two tests are not that far apart from each other as the original intent and that will have to be leveraged in the results discussion and conclusions. Nevertheless, a secondary objective of the work is to characterize the 42CrMo4 material behaviour at high temperature forging (1370 °C) and this exercise apart from analysing the impact between those two deformation-states will provide that information.

Fig. 14 schematically represents the methodology followed in this section. From left to right:

Phase A.

1. Compression tests of 42CrMo4 material under high temperature conditions are conducted.
2. Experimental data from these compression tests are used as a reference for an inverse numerical analysis. This analysis calibrates a Hansel-Spittel model that represents the compression behaviour of the material.

Phase B.

1. Plane strain compression tests are conducted using the same material and temperature conditions as the compression tests.
2. The numerical model, fed with the previously calibrated Hansel-Spittel model (step 2), is used for blind predictions that are compared with the experimental data from the plane strain compression tests.

This comparative analysis aims to evaluate if significant differences exist in characterizing the material under uniaxial compression mode versus plane strain compression mode. If the simulation of step 4 fails to predict the force displacement data of the plane strain compression test, that means that material models calibrated with compression test are not suitable for different deformation-state driven processes. Nevertheless, if the simulation of step 4, succeeds on predicting the force displacement of the plane strain compression test, that means that both characterization test is exchangeable as this material (42CrMo4) at these specific high temperatures (1370 °C, characteristic of NSF processes). And therefore, the impact of the deformation-state on the material behaviour is neglectable. All this levering the boundary deformation-states of the study.

3.1.1. Experimental methodology- compression test

The compression test is performed using the Gleeble 3800C (max 20 t and 2 m/s) thermomechanical system at SIDENOR I + D, as illustrated on the right side of Fig. 15. A sample of 10 mm in diameter and 15 mm in length has been used. During the test, the billet is positioned between two horizontally aligned plates, with tantalum and graphite foils on each side to prevent sticking. Two R-Type thermocouples are welded to the centre of the billet for heating control. Fig. 15(a) shows the experimental

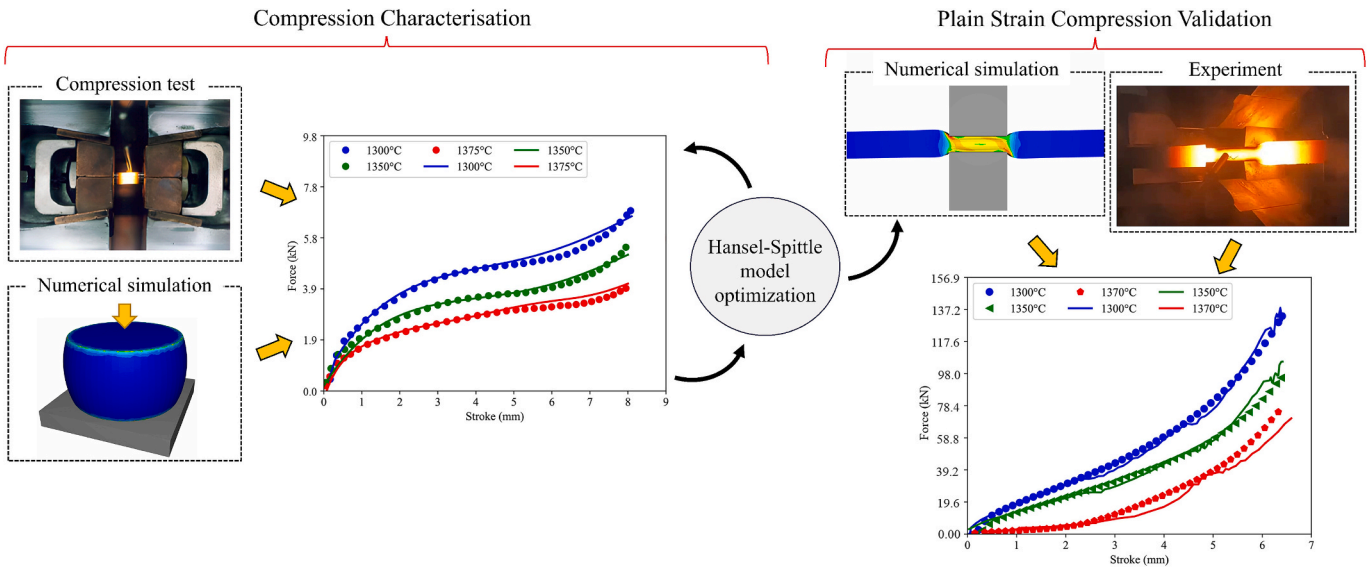

Fig. 14. Schematic representation of characterization methodology.

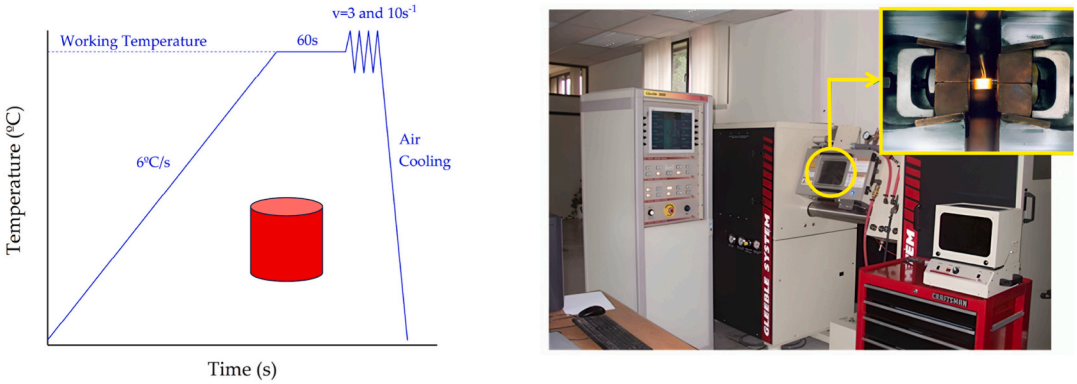

Fig. 15. Compression test method and equipment details.

sequence of the heating cycle during the test performed by Joule heating.

The compression test is conducted at three different temperatures: 1300 °C, 1350 °C, and 1375 °C. These temperatures were chosen based on the manufacturing conditions of the NSF process. The test involves a heating rate of 6 °C/s followed by a homogenization stage. Deformation is then performed at stroke speeds equivalent to averaged strain rates of 1 s^{-1} and 10 s^{-1}, which are typical for high-speed deformation in the industrial process.

3.1.2. *Experimental methodology- plane strain compression test*

Compression tests were performed at the Advanced Steel Research

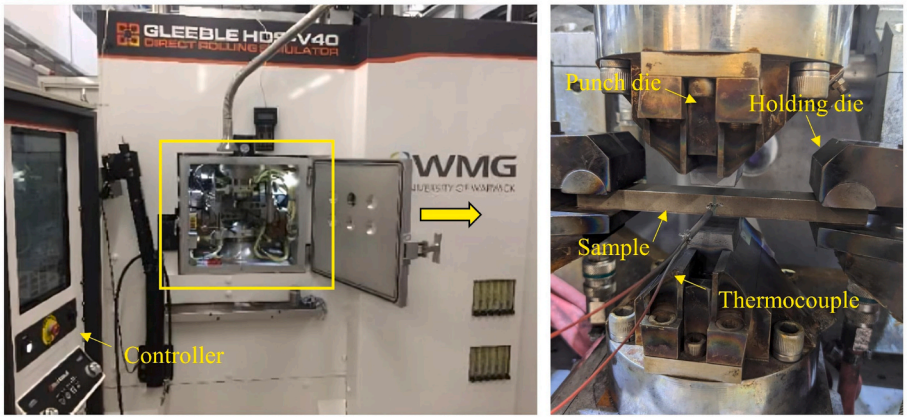

Fig. 16. Plane strain compression test equipment details.

Centre in the University of Warwick employing the HDS-V40 thermo-mechanical Gleeble system (Fig. 16). The Gleeble system has a loading capacity of 40 tons and can reach a stroke rate of 1.7 m/s. The sample heating is performed through Joule heating. Rectangular samples with dimensions of 140 mm x 20 mm x 10 mm were used for the tests. The top surfaces of the samples were maintained parallel and free of flash to prevent hot spots during Joule heating. To prevent the material from sticking to the anvils at high temperatures, graphite and tantalum foils were placed on each side of the samples. Nickel paste was applied, assuring the contact and ensuring efficient power transfer through all elements. The Gleeble heating system uses a closed loop for temperature control. In this case, a C-type thermocouple was placed into two 5 mm deep and 0.7 mm diameter holes (as illustrated in Fig. 16 right side).

Following the same strategy as in the compression test, temperatures of 1300 °C, 1350 °C, and 1370 °C were studied. The test speed was selected to match the averaged strain rate values of 1 and 10 s^{-1}. The punch configuration and the deformation force recorded during the test are shown in Fig. 17(a). This figure illustrates that the sample is pressed and held for 10 s during the experimental tests. Additionally, figure 17 (b) provides a view inside the Gleeble equipment, where the plane strain test sample is compressed between the dies. The final shape of the tested sample is depicted in the bottom right corner of Fig. 17.

3.1.3. Numerical methodology- compression test

In line with section one of the manuscript, to replicate the compression test conducted experimentally, a finite element model is constructed using the FORGE NXT® numerical analysis tool. For a more detailed description of the FEM model please refer to section 2.1.1.

General data of the 42CrMo4 material has been assumed with a density of 7850 kg/m^3 and an elastic modulus of 193 GPa with a Poisson ratio of 0.29 [33]. The plastic behaviour of the material is described using the Hansel–Spittel model, which defines the relationship between flow stress, strain, strain rate, and deformation temperature [34]. The Hansel–Spittel model is represented by the following equation:

$$\sigma = Ae^{m_1 T}\varepsilon^{m_2}\dot{\varepsilon}^{m_3}e^{\frac{m_4}{\varepsilon}}(1+\varepsilon)^{m_5 T}e^{m_{7\varepsilon}}\dot{\varepsilon}^{Tm_8}T^{m_9} \quad (1)$$

where σ is stress, ε is strain, $\dot{\varepsilon}$ is strain rate, T is deformation temperature and m_1 to m_9 are material constants. m_1 is the coefficient for temperature correlation; m_2 is the index for strain strengthening; m_3 is the index for strain-rate strengthening; m_4 is the coefficient for strain softening; m_5 indicates the coupling coefficient for temperature and strain; m_7 is the coefficient for strain strengthening; m_8 indicates the coupling coefficient for strain rate and temperature; and m_9 is the index for temperature strengthening.

To optimize the model parameters in the Hansel–Spittel model, a generalized reduced gradient (GRG) nonlinear method was implemented. This method is commonly used to solve nonlinear problems and calculate the local optimal solution. Initially, the error in the numerical flow stress was calculated relative to the experimental data. The GRG method was then used to minimize these error values. A total of 5000 iterations were performed to achieve the appropriate values of the fitted parameters.

3.1.4. Numerical methodology- plane strain compression test

A finite element model of the plane strain compression test is constructed using the FORGE NXT® numerical analysis tool following the same strategy as in section 1 of the manuscript. Refer to that section 3.1.3 for a more detailed description of the model.

3.2. Results and discussion on the impact of the deformation-state on the material behaviour

As stated in section 3.1.3 and schematically shown in Fig. 14, the second step of Phase A of the process is to obtain the set of parameters of the material model that lead to the correct prediction of force displacement data compared to the experimental.

After the GRG iterative process, the optimum data set has been retrieved, and these parameters are presented in Table 1.

In addition, Fig. 18 shows the prediction accuracy using these parameters against the experimental. In a continuous line the numerical model prediction is presented while experimental data is shown in markers. Two distinct graphs (Fig. 18a and b) are composed each for a different equivalent strain rate and the results of the studied three temperatures are presented.

Fig. 19 depicts the distribution of effective stress during the compression test across all tested temperatures. The results reveal that higher stress levels were consistently observed at a strain rate of 10 s^{-1} compared to 1 s^{-1}. Furthermore, temperature variations also influenced the stress distribution, with lower temperatures showing higher stress values compared to the highest temperature of 1375 °C. This highlights the sensitivity of stress levels to both strain rate and temperature during the compression test, reflecting the dynamic nature of material response under high temperature conditions.

Once that the Phase A is complete, steps 3 and 4 of Phase B are conducted and in the following lines the results and discussion of the procedure are presented (section 3.1.3 and Fig. 14). Taking the material parameters presented in Table 1, the plane strain compression simulation (depicted in section 3.1.4) is conducted. The output of that blind simulation is then compared to the experimental force displacement data obtained from the experiments (section 3.1.2). Fig. 20 shows the blind prediction against experimental for the plane strain compression data. In the continuous line, the blind prediction of the model, feed with compression calibrated data, is presented while the plane strain compression experiment is shown in markers.

Upon detailed examination, a close correlation between the

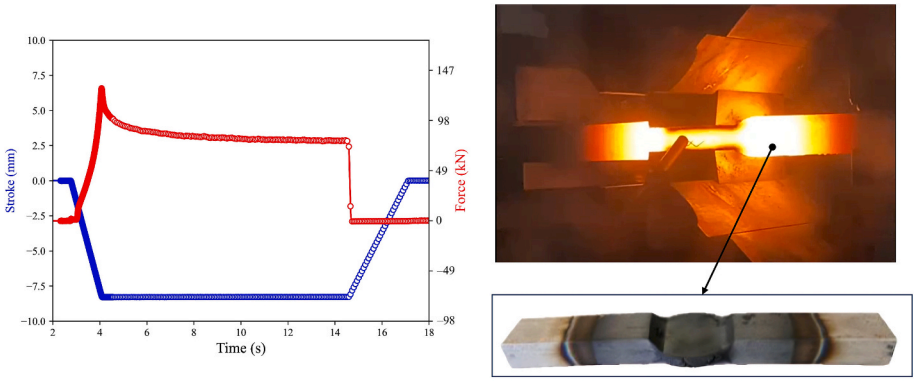

(a) Punch configuration

(b) Tested sample

Fig. 17. Plane strain compression testing: (a) Punch configuration and forces at 1300 °C (b) Testing phase.

Table 1
Modified Hasel spittle model parameters.

A	m_1	m_2	m_3	m_4	m_5	m_6	m_7	m_8	m_9
1872.06	$-6.76E^{-03}$	0.4606	0.02341	$-2.42E^{-03}$	$-7.57E^{-04}$	0.00	0.60	$-2.50E^{-05}$	0.8283

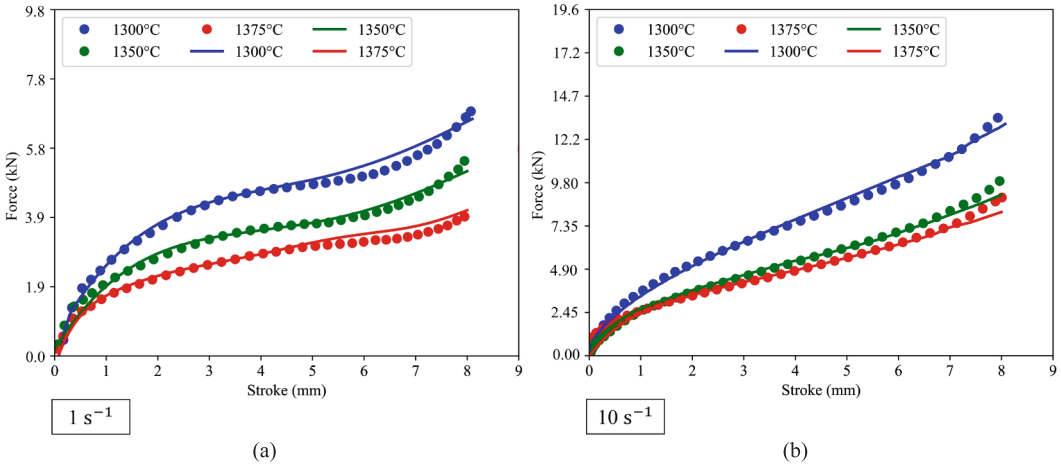

Fig. 18. Numerical model accuracy in the compression test at T = 1300, 1350 and 1375 °C: (a) Strain rate 1 s^{-1} (b) Strain rate 10 s^{-1}.

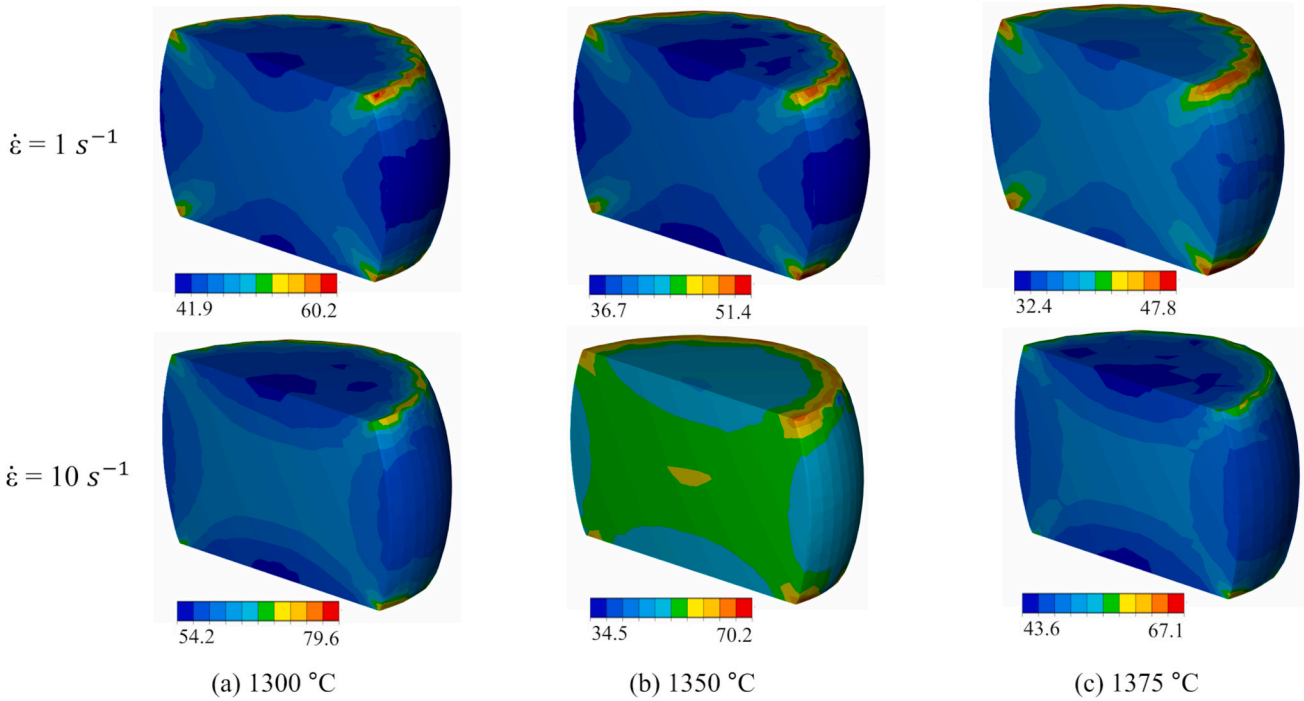

Fig. 19. Effect of temperature and strain rate at stress distribution in the compression test.

numerical and experimental forces is evident. As expected, the temperature significantly affects the forces in the plane strain test. At 1 s^{-1} the maximum force is recorded 137.2 kN at 1300 °C, while a force of 63.7 kN is observed at 1370 °C under the same strain rate. Similarly at 10 s^{-1}, the peak force is recorded at 1300 °C maxing around 68.6 kN, whereas 56.8 kN and 39.2 kN of peak forces are recorded at 1350 °C and 1370 °C respectively. However, minor deviations between experimental and simulation forces are observed at end of the deformation stroke at 1370 °C. Furthermore, a decrease in flow force with increasing strain rate (from 1 s^{-1} to 10 s^{-1}) is recorded in this test. Which is primarily attributed to the high forming temperatures close to the solidus of 42CrMo4 steel (1300–1370 °C). At this elevated temperature, the billet lose heat rapidly during slower deformation, leading to locally lower temperatures and correspondingly higher flow stresses. Conversely, at higher strain rates the deformation occurs faster which reduces the time for heat loss and maintaining a higher billet temperature, which results in lower measured forces. Overall, the model calibrated with compression tests, accurately predicts the force distribution nature observed in the plane strain tests.

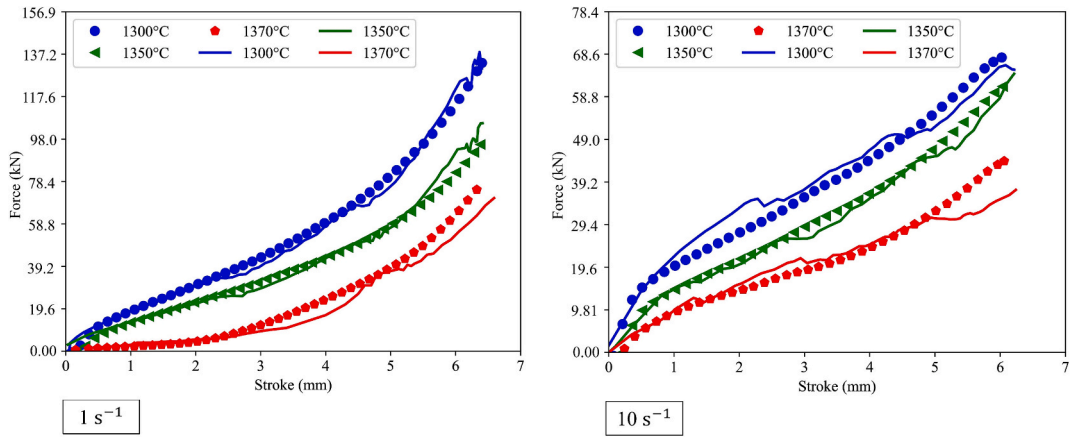

Fig. 20. Experimental and predicted forces using modified Hansel-Spittel model at T = 1300, 1350, 1370 °C and strain rate 1 and 10 s^{-1}.

3.3. Conclusions of research question ②

In this section the main conclusions of the answer to the following question are summarised: ② *do materials (specially 42CrMo4 steel) behave differently under shear deformation at high temperatures compared to compression; and therefore, material models identified based solely on compression tests, can they reliably predict behaviour in high temperature conditions when other deformation-states dominates?*

The first rough answer to this, and a limitation of this work, is that we do not know, as no sample was found suitable for an adequate shear material characterization. From a more constructive point of view, a good agreement between the material characterization at 'compression deformation-state' and 'plane strain compression deformation-state' has been found. Therefore, leading to the conclusion that the deformation-state difference between both test Figs. 9b and 11b do not have a significant impact in the material behaviour for the studied material and strain rate and temperature ranges.

A bonus added value is the parameter set shown in Table 1 that represents the material behaviour of the 42CrM4 calibrated by Hansel-Spittel model for a range of temperature between 1300 °C and 1370 °C in a range of 1 s^{-1} and 10 s^{-1}. This is a highly valuable information for numerical representation of high temperature forging processes, particularly NSF processes.

A drawback or limitation of this section, which leads to an open research gap, is the existence of testing samples suitable for shear characterizations, in which the global deformation energy is really driven by the desired deformation-state. Related with that, a clear limitation of this study is the closeness between deformation-states between compression and plane strain compression. Therefore, the study will have to be extended by future authors opening the triaxiality ranges to other cases.

4. Conclusion

This manuscript, organized in two distinct chapter, gives answer to the following key open questions: ① what is the predominant/driving deformation-state for each state-of-the-art material characterization samples? ② do materials (specially 42CrMo4 steel) behave differently under shear deformation at high temperatures compared to compression; and therefore, material models identified based solely on compression tests, can they reliably predict behaviour in high temperature conditions when other deformation-states dominates?

5. Statements

After presenting conclusions to each chapter now global statements will be given:

- It is of critical importance the accurate analysis of the deformation-state contribution for each sample. In this regard, both compression and plane strain compression samples have been found to be closely representative of their theoretical purpose. On the contrary, all seven studied state-of-the-art shear samples fail to be representative of the expected deformation-state.
- The 42CrMo4 steel material behaviour, in the range between 1300 °C and 1370 °C and 1 s^{-1} and 10 s^{-1} of strain rate is not influenced by the deformation-state difference between compression test and plane strain compression test.
- A suitable set of parameters of the Hansel-Spittle model (Table 1) have been found to model the material behaviour of the 42CrMo4 steel in the detailed range.

6. Limitation

As important as the statements is to clarify the limitation of the study and therefore of the obtained conclusions.

- The inconsistency of deformation-state under state-of-the-art shear samples has been only evaluated with the seven geometries presented in Fig. 5. A different literature geometry could lead to a different massive analysis.
- The driving deformation-state analysis has been conducted with a specific hot forging material from the database and in an specific range of temperatures and deformation speeds. The outcome of the study could vary under different conditions.
- The influence of the deformation behaviour has been studied with a limited range of triaxiality variation (characteristic of compression and plane strain compression tests). Therefore, the stated conclusions are only valid for those ranges. The study of a larger range could lead to a different outcome.
- The impact of the deformation-state on the material behaviour has been studied within a specific range of temperatures and strain rates. A different material and/or temperature and strain rate could lead to different output.

7. Open question/gaps

The following open questions or research gaps have been identified:

- A new shear geometry that leads to a predominant/driving deformation-state close to pure shear, for high temperature material behaviour characterizations remains a challenge. Future strategies include adjusting the aspect ratios of the samples (length to width or height to thickness) to minimize the uniaxial tension and plain strain stresses. Also, other techniques such as reducing the contact distance

between the gauge section to the dies, which can help maintain a more uniform shear deformation across the gauge section. Lastly incorporating notches or dog bone shapes to localize shear and reduce the stress gradients [35–37].
- The extension of the study to other scenarios addressed in the limitation section.

Overall, the research work addresses some key open questions in the high temperature forging community, with a particular focus on the NSF process modelling and optimization. On the one hand, the obtained results give light to some scientific open issues, such as the driving deformation behind each testing methodology/sample and impact of deformation-state in material behaviour. On the other hand, this work also generates valuable insightful knowledge for the digital twin/ numerical representation of high temperature forging, especially NSF. This will be of critical importance on the development of this sustainable manufacturing technology addressing the United Nations sustainable development goal for industry, innovation and infrastructure.

8. Author agreement

We declare that this manuscript entitled "Impact of Triaxiality on Material Behaviour Characterization in Hot Forging Processes: Focus on Near Solidus Forming" is original, has not been published before and is not currently being considered for publication elsewhere.

We confirm that the manuscript has been read and approved by all named authors and that there are no other persons who satisfied the criteria for authorship but are not listed. We further confirm that the order of authors listed in the manuscript has been approved by all of us.

We understand that the Corresponding Author is the sole contact for the Editorial process. He is responsible for communicating with the other authors about progress, submissions of revisions and final approval of proofs.

Declaration of generative AI and AI-assisted technologies in the writing process

During the preparation of this work the author(s) used Chat GTP Open AI 3.5 for the re-write of the text to improve its quality. After using this tool, the author(s) reviewed and edited the content as needed and take(s) full responsibility for the content of the publication.

10. Data Availability Statement

All data supporting the findings of this study are included within the paper and its Supplementary Information. Additional data if required, are available from the corresponding author upon request.

CRediT authorship contribution statement

Muhammad Sajjad: Writing – original draft, Visualization, Validation, Software, Methodology, Investigation, Formal analysis. **Julen Agirre:** Methodology, Investigation, Formal analysis. **Gorka Plata:** Conceptualization, Methodology, Investigation, Writing – review & editing. **Jokin Lozares:** Conceptualization, Methodology, Investigation, Writing – review & editing, Resources. **Carl Slater:** Methodology, Investigation, Formal analysis. **Joseba Mendiguren:** Conceptualization, Resources, Supervision, Project administration, Writing – review & editing.

Declaration of competing interest

The authors declare that they have no known competing financial interests or personal relationships that could have appeared to influence the work reported in this paper.

Acknowledgments

The authors would like to acknowledge the Exploration of high entropy alloys as substitute materials for sustainable mobility and decarbonisation (HEAPLAS) project funded by Ministerio de Ciencia e Innovación, with the reference PID2022-139130OA-I00, the HSSF, Hybrid Semi-Solid Forming project funded by the "Research Fund for Coal and Steel" (RFCS) program of the European union, with the grant number 800763, and the Procesos de Fabricación de Excelentes para propiedades máximas (PROMAX), funded by Basque Government through the ELKARTEK funding scheme (reference KK-2020/00087).

Data availability

Data will be made available on request.

References

[1] E.J. Zoqui, Alloys for semisolid processing, in: Comprehensive Materials Processing, Elsevier, 2014, pp. 163–190, https://doi.org/10.1016/B978-0-08-096532-1.00520-3.
[2] J. Lozares, G. Plata, I. Hurtado, A. Sánchez, I. Loizaga, Near solidus forming (NSF): semi-solid steel forming at high solid content to obtain as-forged properties, Metals (basel) 10 (2020) 198, https://doi.org/10.3390/met10020198.
[3] D. Abedul, L. Galdos, E. Sáenz de Argandoña, F. Galvez, B. Erice, Effect of the loading-rate and stress state on the constitutive modelling and fracture of 2205 Duplex stainless steel, Int. J. Impact Eng 191 (2024) 104991, https://doi.org/10.1016/j.ijimpeng.2024.104991.
[4] M. Sajjad, J. Trinidad, G. Plata, J. Lozares, J. Mendiguren, Sensitivity analysis of near solidus forming (NSF) process with digital twin using Taguchi approach, Adv. Manuf. 13 (2025) 322–336, https://doi.org/10.1007/s40436-024-00482-4.
[5] C.C. Roth, D. Mohr, Determining the strain to fracture for simple shear for a wide range of sheet metals, Int. J. Mech. Sci. 149 (2018) 224–240, https://doi.org/10.1016/j.ijmecsci.2018.10.007.
[6] M. Sajjad, J. Agirre, G. Plata, J. Lozares, J. Mendiguren, Characterization of friction coefficient at near solidus forming (NSF) conditions using t-shape compression test, J. Manuf. Process. (2024), https://doi.org/10.1016/j.jmapro.2024.07.009.
[7] M. Sajjad, J. Agirre, G. Plata, J. Lozares, J. Mendiguren, Characterization of the heat transfer coefficient (HTC) at near solidus forming (NSF) condition using columnar pressing test, Int. J. Adv. Manuf. Technol. (2024), https://doi.org/10.1007/s00170-024-14531-6.
[8] G. Plata, J. Lozares, A. Sánchez, I. Hurtado, C. Slater, Preliminary study on the capability of the novel near solidus forming (NSF) technology to manufacture complex steel components, Materials 13 (2020) 1–14, https://doi.org/10.3390/ma13204682.
[9] C. Slater, G. Plata, A. Sánchez, J. Lozares, I. Hurtado, A novel forming technique to coforge bimetal components into complex geometries, Manuf. Lett. 26 (2020) 21–24, https://doi.org/10.1016/j.mfglet.2020.09.006.
[10] S.-J. Park, K. Lee, B.C. Cerik, J. Choung, Ductile fracture prediction of EH36 grade steel based on Hosford–Coulomb model, Ships Offshore Struct. 14 (2019) 219–230, https://doi.org/10.1080/17445302.2019.1565300.
[11] S. Gao, Y. Sang, Q. Li, Y. Sun, Y. Wu, H. Wang, Constitutive modeling and microstructure research on the deformation mechanism of Ti-6Al-4V alloy under hot forming condition, J. Alloys Compd. 892 (2022) 162128, https://doi.org/10.1016/j.jallcom.2021.162128.
[12] Y. Lou, J.W. Yoon, H. Huh, Q. Chao, J.-H. Song, Correlation of the maximum shear stress with micro-mechanisms of ductile fracture for metals with high strength-to-weight ratio, Int. J. Mech. Sci. 146–147 (2018) 583–601, https://doi.org/10.1016/j.ijmecsci.2018.03.025.
[13] C.C. Roth, T. Tancogne-Dejean, D. Mohr, Plasticity and fracture of cast and SLM AlSi10Mg: High-throughput testing and modeling, Addit. Manuf. 43 (2021) 101998, https://doi.org/10.1016/j.addma.2021.101998.
[14] B. Kowalski, C.M. Sellars, M. Pietrzyk, Identification of rheological parameters on the basis of plane strain compression tests on specimens of various initial dimensions, Comput. Mater. Sci 35 (2006) 92–97, https://doi.org/10.1016/j.commatsci.2005.02.024.
[15] A. Hor, F. Morel, J.-L. Lebrun, G. Germain, An experimental investigation of the behaviour of steels over large temperature and strain rate ranges, Int. J. Mech. Sci. 67 (2013) 108–122, https://doi.org/10.1016/j.ijmecsci.2013.01.003.
[16] K. Zhang, H. Badreddine, N. Hfaiedh, K. Saanouni, J. Liu, Enhanced CDM model accounting of stress triaxiality and Lode angle for ductile damage prediction in metal forming, Int. J. Damage Mech 30 (2021) 260–282, https://doi.org/10.1177/1056789520958045.
[17] M.B. Gorji, D. Mohr, Micro-tension and micro-shear experiments to characterize stress-state dependent ductile fracture, Acta Mater. 131 (2017) 65–76, https://doi.org/10.1016/j.actamat.2017.03.034.
[18] F. Khameneh, A. Abedini, C. Butcher, Lengthscale effects in optical strain measurement for fracture characterization in simple shear, Int. J. Fract. 232 (2021) 153–180, https://doi.org/10.1007/s10704-021-00598-9.
[19] F. Andrade, S. Conde, M. Feucht, M. Helbig, A. Haufe, Estimation of Stress Triaxiality from optically measured Strain Fields, 2019.

[20] Z.A. Mehari, J. Han, Numerical prediction of ductile fracture during the partial heating roll forming process of DP980, Int. J. Fract. 234 (2022) 97–112, https://doi.org/10.1007/s10704-021-00572-5.
[21] L. Driemeier, M. Brünig, G. Micheli, M. Alves, Experiments on stress-triaxiality dependence of material behavior of aluminum alloys, Mech. Mater. 42 (2010) 207–217, https://doi.org/10.1016/j.mechmat.2009.11.012.
[22] J.R. Rice, D.M. Tracey, On the ductile enlargement of voids in triaxial stress fields*, J. Mech. Phys. Solids 17 (1969) 201–217, https://doi.org/10.1016/0022-5096(69)90033-7.
[23] F.A. McClintock, Local criteria for ductile fracture, Int. J. Fract. Mech. 4 (1968) 101–130, https://doi.org/10.1007/BF00188939.
[24] F. Rickhey, S. Hong, Stress triaxiality in anisotropic metal sheets—definition and experimental acquisition for numerical damage prediction, Materials 15 (2022) 3738, https://doi.org/10.3390/ma15113738.
[25] J. Zhang, D. Wu, J. Zhou, J. Wang, Multi-objective optimization of process parameters for 7050 aluminum alloy rib-web forgings' precise forming based on Taguchi method, in: Procedia Eng, Elsevier Ltd, 2014: pp. 558–563. https://doi.org/10.1016/j.proeng.2014.10.039.
[26] H. Li, W. Jiao, H. Feng, X. Li, Z. Jiang, G. Li, L. Wang, G. Fan, P. Han, Deformation characteristic and constitutive modeling of 2707 hyper duplex stainless steel under hot compression, Metals (basel) 6 (2016) 223, https://doi.org/10.3390/met6090223.
[27] O. Bilbao, I. Loizaga, J. Alonso, F. Girot, A. Torregaray, 42CrMo4 steel flow behavior characterization for high temperature closed dies hot forging in automotive components applications, Heliyon 9 (2023) e22256, https://doi.org/10.1016/j.heliyon.2023.e22256.
[28] M. Pop, I.-M. Sas-Boca, D. Frunză, F. Popa, A. Neag, The influence of hot deformation on the mechanical and structural properties of 42CrMo4 steel, Metals (basel) 14 (2024) 647, https://doi.org/10.3390/met14060647.
[29] M. Sajjad, J. Trinidad, G. Plata, J. Lozares, J. Mendiguren, Sensitivity analysis of near solidus forming (NSF) process with digital twin using Taguchi approach, Adv. Manuf. (2024), https://doi.org/10.1007/s40436-024-00482-4.
[30] C. Slater, N. Tamanna, C. Davis, Optimising compression testing for strain uniformity to facilitate microstructural assessment during recrystallisation, Result. Mater. 11 (2021) 100218, https://doi.org/10.1016/j.rinma.2021.100218.
[31] S. Cooreman, D. Lecompte, H. Sol, J. Vantomme, D. Debruyne, Elasto-plastic material parameter identification by inverse methods: Calculation of the sensitivity matrix, Int. J. Solids Struct. 44 (2007) 4329–4341, https://doi.org/10.1016/j.ijsolstr.2006.11.024.
[32] M. Bäker, A. Shrot, Inverse parameter identification with finite element simulations using knowledge-based descriptors, Comput. Mater. Sci 69 (2013) 128–136, https://doi.org/10.1016/j.commatsci.2012.11.059.
[33] Julia B, Modeling the link between microstructure, thermomechanical treatment and mechanical performance of refractory products, Université Grenoble Alpes, 2022.
[34] K. Chadha, D. Shahriari, M. Jahazi, An approach to develop hansel–spittel constitutive equation during ingot breakdown operation of low alloy steels, in: Frontiers in Materials Processing, Applications, Research and Technology, Springer Singapore, Singapore, 2018, pp. 239–246, https://doi.org/10.1007/978-981-10-4819-7_20.
[35] Z. Xie, W. Wang, Z. Yao, Experiments and modeling of shear ultra-low-cycle fatigue of structural steel considering plastic deformation histories, Constr. Build. Mater. 418 (2024) 135409, https://doi.org/10.1016/j.conbuildmat.2024.135409.
[36] Y. Bao, T. Wierzbicki, On fracture locus in the equivalent strain and stress triaxiality space, Int. J. Mech. Sci. 46 (2004) 81–98, https://doi.org/10.1016/j.ijmecsci.2004.02.006.
[37] B. Starman, B. Chen, A. Maček, Y. Zhang, M. Halilovič, S. Coppieters, Characterising through-thickness shear anisotropy using the double-bridge shear test and finite element model updating, Materials 18 (2025) 2220, https://doi.org/10.3390/ma18102220.